CHAPTER 1

Introduction: A bibliographic review

1.1 Introduction

The major pursuit of condensed matter physics is to find out the new phases of matter to keep the perpetual progress and developments in electronic devices. According to the band theory of solids, conventionally, three types of materials exist; metal, semiconductor and insulators. These three can be classified on the basis of bandgap, and a simple picture of band diagram can be seen in figure 1.1, where conduction band and valance band is associated with the upper and lower energy states, respectively. The size of the energy gap between the conduction band and valance band governs the nature of the material, whether it is conductor, insulator or semiconductor. In conductors, the conduction band and valance band are overlapped. Therefore, the valance electrons can move freely in the conduction band and participate in conduction. In insulators, the conduction band and valance band is far away from each other (bandgap > 5eV), and this gap prevents electrons from participating in conduction. Semiconductors have the intermediate properties of conductors and insulators.

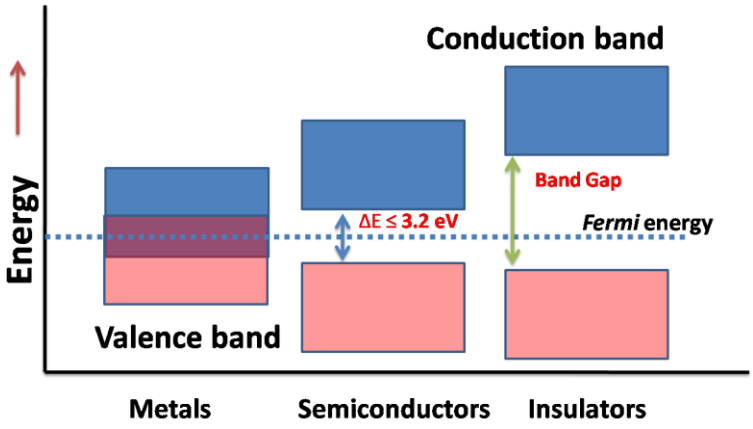

Figure 1.1: Band diagram for metal, semiconductor and insulator

The discovery of the Quantum Hall Effect introduces a new state of quantum matter that possesses a conducting surface state with the existence of a bulk insulating phase known as the Topological Insulator[1], [2]. Topological Insulators have grabbed a lot of interest of the science fraternity because it may serve as a platform for fundamental physics phenomena and potential technological applications such as quantum computing and spintronics [1]. 3D topological Insulators lead the gapless conducting surface states (SS), topologically protected by Time Reversal symmetry (TRS)[1], [3]. The existence of the coupling of the spin and orbital angular momentum of an electron leads to a band inversion phenomenon in TIs[4], [5]. Due to spin-orbit coupling (SOC), the spin-momentum are locked perpendicularly since the spin-momentum locking at the surface is protected by TRS, which protects the surface states from backscattering by nonmagnetic impurities as well as antisite defects[1], [5]. As a result, the electrical conduction at the edge and surface becomes robust against backscattering which induces a lot of fascinating properties. TIs serve as a platform to the possibility of Majorana fermions which are their antiparticles itself and can be used in quantum computing, whereas magnetic TIs may induce the magnetic monopoles and exhibit the quantum phenomena in the system[1], [2]. There are other intriguing properties like exciton condensation, quantum anomalous Hall effect (QAHE), topological Hall effect (THE), topological superconductivity, which are favorable for application in quantum computing and spintronics devices[6], [7]. It is theoretically established that the topological surface state (TSS) of TIs have a linear energy-momentum relation which leads Aharonov-Bohm oscillations, weak antilocalization (WAL) effect and quantum conductance fluctuation in the system[8], [9]. All of them are associated with the topological surface state (TSS) as well as SOC inserts a band inversion at the gamma point ($\bar{\Gamma}$) near Fermi level (E_f). Due to this, magnetotransport properties becomes very interesting. Moreover, the linear dispersion on the

spin-polarised surface state leads the relativistic Dirac fermions to become relevant. The variety of effects can be explored by doping magnetic or nonmagnetic impurity. For example, TRS can be destroyed at the Dirac point (DP) by the magnetically doped TIs and make the Fermi level tunable. The tunable Fermi level plays an important role to operate the surface transport properties. 2D and 3D topological insulators have been predicted theoretically and later experimentally realized. To understand topological insulators, it is essential to understand the idea of topology.

1.2 Topology

Topology is a mathematical study of the properties that remains invariant through smooth deformation, twisting and stretching of objects. However, tearing and gluing are not allowed. A property that remains invariant is called topological property. Suppose two geometrical constructions undergo smooth deformations and transform into one another, called topologically equivalent. The basic example of topology is coffee mug and doughnut. The coffee mug goes under a smooth deformation and turns into a doughnut which is shown in figure 1.2.

Figure 1.2: Schematic representation of topology showing smooth deformation from cup to doughnut.

However, an apple can't be deformed into a doughnut. In mathematics, the Gauss-Bonnet theorem connects the curvature (geometry) of the surface to their topology and correlates it to the genus of the object;

$$\frac{1}{2\pi}\oint K.dA = x \tag{1.1}$$

Where χ is quantized and associated with the genus g, according to the relation χ = 2-2g. g is related to the no. of holes in an object. Geometries that have equal no. of holes are topological equivalent. For instance, a coffee mug has g = 1, like a doughnut, while a sphere has g = 0; therefore, the doughnut and sphere are topologically distinct. Thus, the two objects having a similar value of genus can be smoothly transformed to each other and have the same topological properties.

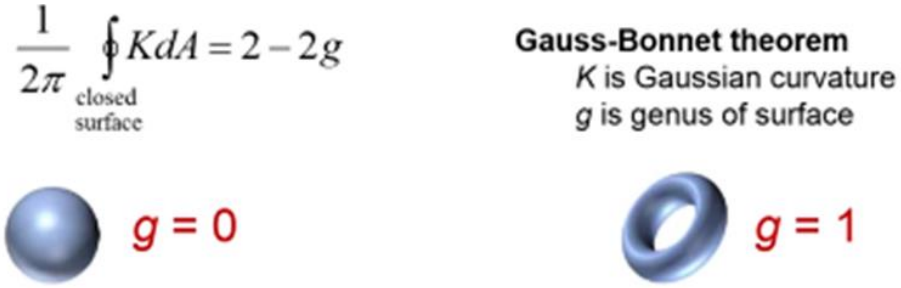

Figure 1.3: The sphere and the doughnut are topologically non-equivalent and have different genus numbers.

By the topology theory, one can classify the phases of matter and, particularly, characterize the insulators. An insulator is defined by the bandgap between the conduction and valance band. Two insulators can be said topologically equivalent if they can be deformed into each other by changing their Hamiltonian adiabatically.

The main feature to specify the state of the matter regarding topological classification is defined by the Berry phase.

1.3 Berry Phase and Chern number

In solids, various phenomena can be understood by the Berry phase. In crystalline solids, the wave vector K is periodic in the Brillouin zone (BZ). This geometric phase is associated with the Bloch wave function $|u_m(K)>$, where K denotes momentum in the BZ. Such Berry phase can be defined by the varying Bloch function in the BZ. In general, the Berry phase may be expressed by the line integral;

$$A_m(\mathrm{K}) = \mathrm{i} < u_m|\Delta \mathrm{k}|u_m > \tag{1.2}$$

Where, A_m is a vector (in term of Bloch wavefunction). The surface integral of Berry curvature is;

$$F_m(\mathrm{K}) = \Delta_k \times A_m(\mathrm{K}) \tag{1.3}$$

The total Berry Flux in BZ may be expressed;

$$\mathrm{n} = \frac{1}{2\pi} \oint_{\mathrm{BZ}} \mathrm{d}^2\mathrm{k}\ F_m(\mathrm{K}) \tag{1.4}$$

Here n is an integer, known as Chern number. The Chern number is a topological invariant provided when the Hamiltonian varies smoothly. According to Hasan and Kane, when n = 0, an insulator is trivial and if n = 1, it relates to quantum spin hall insulator [1]. A trivial insulator has a gapped edge state, but a nontrivial insulator has a gapless helical edge state, unlike the trivial Insulator.

1.4 Time-Reversal Symmetry (TRS)

We can understand TIs by the concept of order, which is very common in condensed matter physics. Generally, the phases of matter such as solid, liquid can be understood in terms of symmetry. Landau theory of phase transition explained that these transitions occur due to symmetry breaking. In a crystal, translational symmetry is broken, and rotational symmetry is broken during the phase transition of liquid. Other complex phases are achievable by symmetry braking, such as ferromagnetic (rotational symmetry breaking) and

superconducting (broken gauge symmetry). But, the beauty of the topological insulator is the preservation of symmetry, and this is the time-reversal symmetry. The topological SS is always protected by time-reversal symmetry (TRS). Due to TRS the edge (2D) and surface (3D) state of TIs become robust against nonmagnetic impurity or defects; therefore, no backscattering occurs in these states. The absence of backscattering at the SS of TIs is a result of spin momentum locking. Electrons can move only in the forward direction due to strong spin-orbit coupling (SOC), and no spin state is available for backward direction without flipping its direction because the spin direction of electrons is linearly bounded with its momentum. This property makes TIs attractive, and we can get dissipationless devices and other applications too.

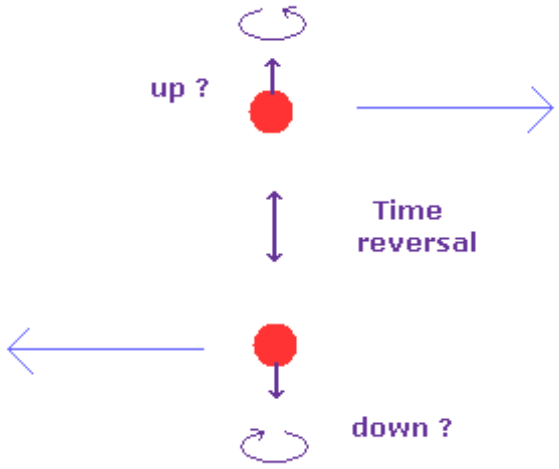

Figure 1.4: Schematic diagram of motion of two electrons having opposite spins with preservation of TRS in TSS.

1.5 Background of Topological Insulator

1.5.1 Hall Effect:

The base of the topological insulator was put at the time of discovery of the Hall effect. Edwin Hall discovered the Hall effect in 1879[10]. When a conducting slab or a metal is

placed in an electric field, and the magnetic field is applied in the perpendicular direction of the electric field, The charge carriers are experienced Lorentz force as well as the electric field force. Due to which equal and opposite charges are accumulated on the opposite faces. As a result, Voltage is created across the conductor known as Hall voltage (V_H), and this phenomenon is known as Hall effect. In figure 1.5, the semantic diagram of the Hall setup has been shown. With the help of Hall effect, one can determine the carrier concentration and also figure out the type of charge carriers.

Let us consider, n-type semiconductor in figure 1.5. Therefore the charge carriers are electron (e^-). The electrons are travelled with the velocity v in the perpendicular direction of the magnetic field. As a result, the Lorentz force eVB is generated. Where e, the charge of e^- and B is the magnetic field in the z-direction. Hence, a negative charge accumulated at the downward face of the conductor; therefore, the potential difference is developed between the bottom and top surface of the slab.

Due to the application of electric field (E_H), a force (eE_H) is applied in the upward direction on the e^- to maintain the equilibrium;

$$E_H = eVB \tag{1.5}$$

$$E_H = VB \tag{1.6}$$

The current density (J_x) in the direction of x can be written as;

$$J_x = neV \tag{1.7}$$

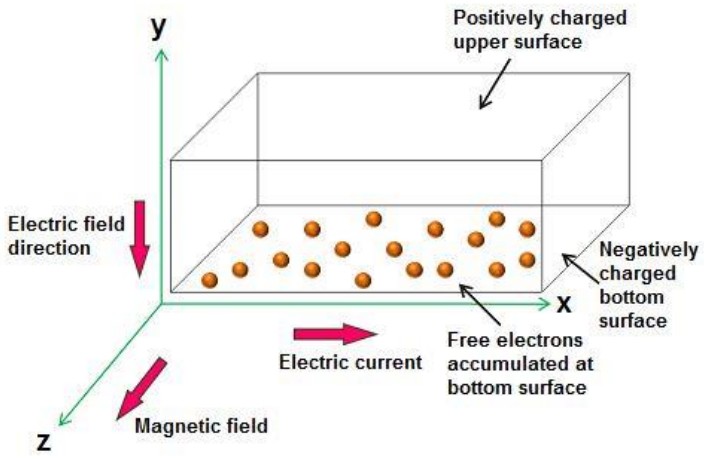

Figure 1.5: Schematic diagram of Hall effect (https://www.physics-and-radio-electronics.com/electronic-devices-and-circuits/semiconductor/halleffect.html)

Where n is the carrier concentration, hence;

$$E_H = \frac{\mathrm{BJ_x}}{ne} \tag{1.8}$$

The Hall coefficient can be defined as;

$$E_H = R_H \mathrm{B} J_x \tag{1.9}$$

$$R_H = \frac{\mathrm{E_H}}{\mathrm{BJ_x}}; \tag{1.10}$$

$$R_H = \frac{1}{n_e} \tag{1.11}$$

In the case of n-type semiconductor;

$$R_H = -\frac{1}{n_e} \tag{1.12}$$

The negative sign indicates that the electric field is developed in negative y-direction therefore, the charge carriers are electrons.

1.5.2 Effect of the magnetic field in 3D system

On application of high magnetic field in a 3D system, it is observed that very intriguing properties are induced in the system, i.e., Quantization of energy level in the form of Landau

Level, oscillations in the electrical resistivity (SdH Oscillations) as well as an oscillation in magnetization (deHass-Van Alphen Effect) and many more. The appearance of oscillations in the resistivity and magnetization is due to the quantization of energy. If the magnetic field is applied along the z-direction (B_z), no force is experienced on the e^- in the direction of the applied magnetic field. Therefore, the motion of e^- (in the z-direction) remains unaffected. According to the quantum harmonic oscillator, the e^- acts as they are free to move in the z-direction while quantized in x and y-direction. The energy of such e^- can be written as;

$$E_n = (n + \frac{1}{2})\,\hbar\omega_c + \frac{\hbar^2 K_z^2}{m_e^*}, \text{ where } n = 0,1,2,3\ldots\ldots \qquad (1.13)$$

Where n is the number of landau level and m_e is the effective mass of e^- K_z is the momentum vector of e^- in z-direction and ω_c represents the frequency of cyclotron and can be understood as;

$$\omega_c = \frac{eB_z}{m_e^*} \qquad (1.14)$$

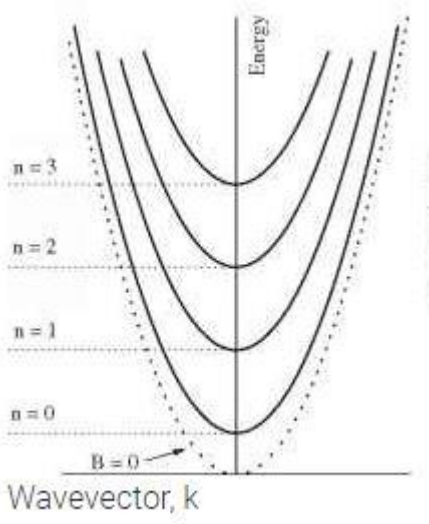

Figure 1.6: Energy band diagram for electrons vs wave vector for different Landau levels in 3D system [https://www.texaspowerfulsmart.com/quantum-wells/chapter-7-1.html]

1.5.3 Effect of the magnetic field in 2D system

When a 2D system is subjected to XY plane and the magnetic field is applied in the z-direction. Hence, the e^- experienced the force in the XY plane. Therefore, the energy levels are quantized and follow the quantum Harmonic oscillator model. The energy of the system can be written as;

$$E_n = (n + \frac{1}{2})\,\hbar\omega_c, \text{ where } n=0,1,2,3\ldots\ldots \quad (1.15)$$

Where n is the no. of landau level and m_e is the effective mass of e^- K_z is the momentum vector of e^- in direction, and ω_c represents the frequency of cyclotron and can be understood as;

$$\omega_c = \frac{eB_z}{m_e^*} \quad (1.16)$$

1.5.4 Quantum Hall Effects (QHE)

The birth of the topological insulator is dedicated to the discovery of QHE. In 1980, Von Klitzing first observed the QHE, when a 2D system was placed under a strong magnetic field and low temperature, then awarded with the novel prize in 1985[1], [11]. The Hall conductance was completely quantized, unlike the classical Hall effect.

$$\sigma_{xy} = n\,\frac{e^2}{h} \quad (1.17)$$

Where n is an integer and h is the Planck's constant and e is the charge of the electron. This phenomenon can be explained in terms of the quantization of e^- motion in the cyclotron orbit. Due to this, the energy levels are also quantized in the landau levels. The energy of Landau levels can be expressed as;

$$E_n = (n + \frac{1}{2})\,\hbar\omega_c \quad (1.18)$$

And

$$\omega_c = \frac{eB}{m} \quad (1.19)$$

Where n is taken as integer, B is perpendicular magnetic field, and m is the electronic cyclotron mass. The Fermi energy lies in between the two Landau levels, and the system behaves like an insulator. The Hall conductivity is completely quantized as expressed in the equation (1.17), and the platue like behaviour can be seen in figure 1.7. There are some intriguing features of QHE that have been listed here.

1) High magnetic field is required.

2) TRS is not preserved.

3) The value of the quantum hall conductance is highly accurate.

4) Longitudinal resistivity (equivalent conductivity) vanishes.

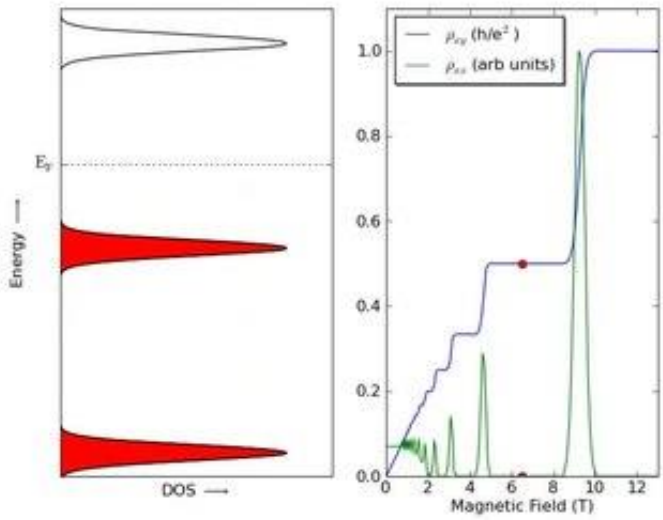

Figure 1.7: Quantization of energy levels into discrete Landau levels under the applied magnetic field (left) and the variation in longitudinal (ρ_{xx}) and transverse resistivity (ρ_{xy}) with applied magnetic field showing QHE. (https://en.wikipedia.org/wiki/Quantum_Hall_effect)

The e$^-$s are moving in a quantized closed circular cyclotron orbit inside the system, initiating insulating behaviour. At the edge, the e$^-$s are allowed to move in the skipping orbits. Therefore, the charge flow at the edge only in a single direction depending on the magnetic field direction. These states belonging to the skipping orbits are known as 'edge states'.

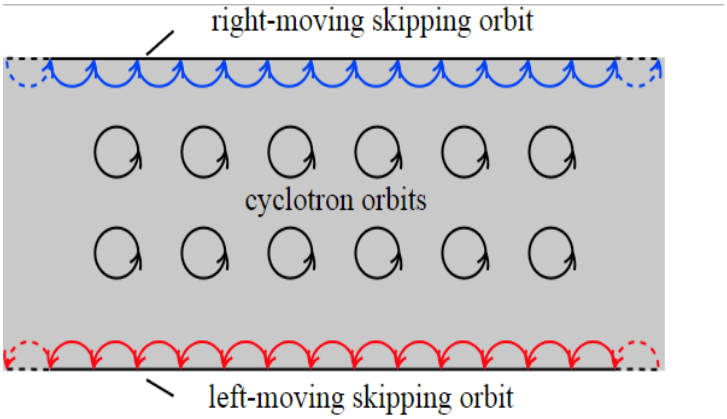

Figure 1.8: Skipping orbits at the edge state and cyclotron orbits in bulk in 2D electron gas in the presence of the magnetic field.

Due to the unidirectional nature of the propagation of charges, the upper and lower edges are chiral. At the edge state, backscattering is not occurred due to the inability of the charge carriers to reverse their direction of motion.

1.5.5 Quantum Spin Hall Effect (QSHE)

The Quantum Spin Hall Effect is the key factor of the 2D topological insulator. After the discovery of QHE, a lot of theoretical works suggested a system having the same conducting properties but without applying an external magnetic field. The TRS is broken in QHE due to the presence of the external magnetic field. The basic difference between QHE and QSHE is that no external magnetic field is needed in QSHE. In fact, the required magnetic field is offered by the internal SOC. Kane, and mele proposed a model in 2005; with the help of this model, the QSHE state can be understood in terms of QHE by taking two copies of QHE with opposite spin and magnetic field which results into QSHE[12].

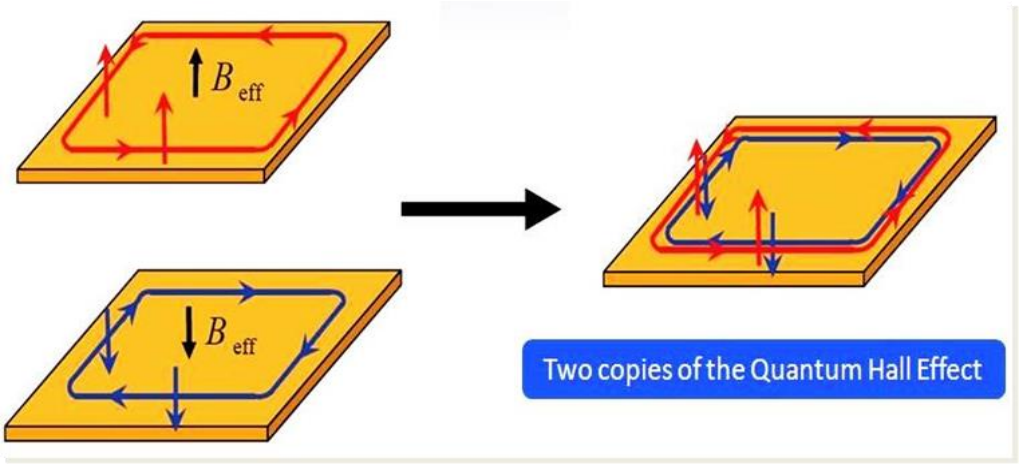

Figure 1.9: Two copies of the quantum Hall effect (QHE) with the opposite magnetic field (left) and (right) the amalgamation of these two QHE states makes a quantum spin Hall effect (QSHE) without applied magnetic field (Adapted from [12]).

Additionally, in QSHE, upper and lower, both the sections of the sample have right and left moving e^- with spin up and down, respectively. These spin-polarized edge states remain unaffected from scattering by the presence of non-magnetic impurity. The propagating e^- does not backscatter, rather than that e^-s detour around the impurity[13] as seen in figure 1.9. Therefore, backscattering is still not allowed in the QSHE if a nonmagnetic impurity or a defect is encountered.

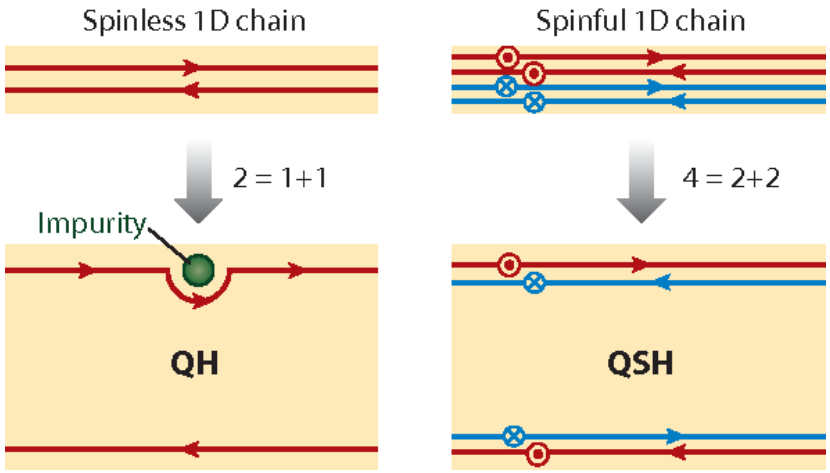

Figure 1.10: (Left) QHE with both right moving and left moving edge states. These states are robust against backscattering. (Right) QSHE with upper state right moving spin up and left moving spin down. Backscattering is suppressed from nonmagnetic impurities (adapted from [13])

When a spin up e^- is encountered with an impurity, the backscattering is possible by two probable ways which is presented in figure 1.11, e^- spin rotates in clockwise and anticlockwise paths around the impurity and creates π and $-\pi$ phase difference, respectively which leads to a 2π path difference overall. Therefore, these two wave functions destructively interfere and lead to dissipationless transport[13]. On introducing a magnetic impurity or applying a magnetic field in TI, TRS is no longer preserved.

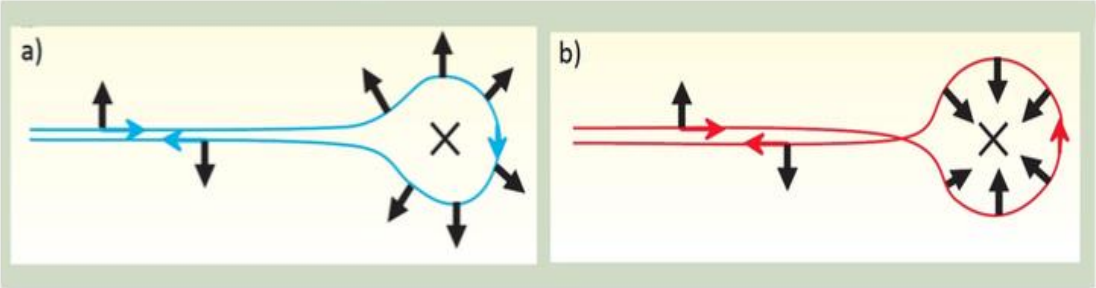

Figure 1.11: schematic diagram of two opposite scattering paths around an impurity for the QSH state. The total path difference between them is 2π, leading to suppression of the backscattering for Fermions (adapted from [13]).

Firstly, Graphene was proposed to have the QSHE, but due to weak SOC of carbon stopped this. The heavy elements have strong SOC. Therefore, they are needed to experience the 2D TIs because SOC is a relativistic term. Bernevig et al., in 2006[15], theoretically predicted that the QSHE might be observed in a HgTe quantum well. A thin layer of HgTe (possess strong SOC) is sandwiched between the two layers of CdTe to make a 2d quantum well structure. After this prediction, in 2007, Konig et al. experimentally observed the quantized conductance of $2e^2/h$ at zero magnetic fields in HgTe. Therefore, HgTe quantum well is known as the first 2D TIs[16].

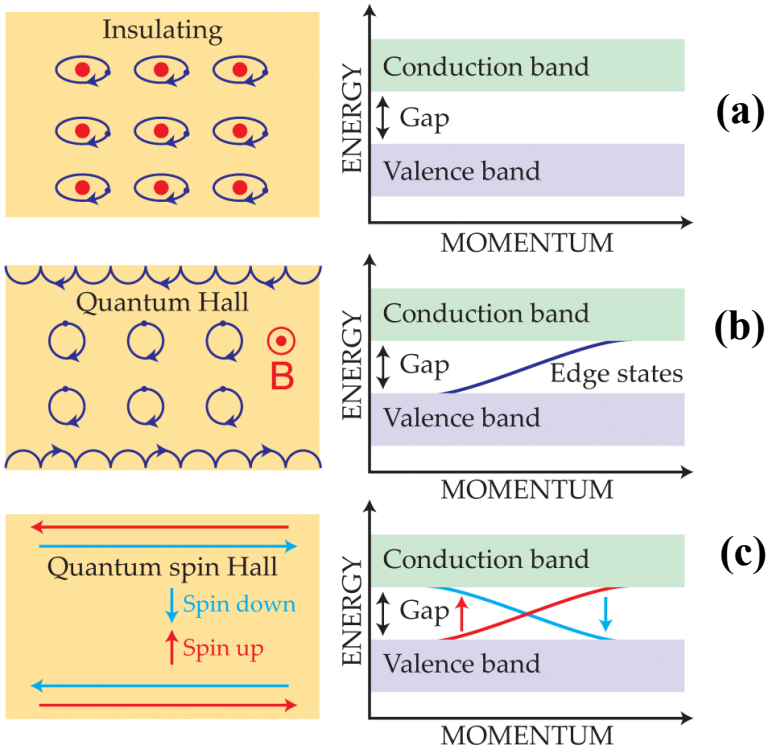

Figure 1.12: schematic diagram of insulating state with a bandgap between the conduction and valence band[14] (b) bulk is insulating but skipping orbits at the edges allows the conduction of electron giving rise to the conduction edge i.e. no band gap[14] (c) in QSHE, both type of left and right moving path having opposite spins are allowed which is protected by time-reversal symmetry[14].

1.5.6 Spin-orbit coupling

When the electron (e^-) spin or intrinsic angular momentum of the e^- interacts with its orbital angular momentum, the SOC arises. In ordinary materials, like semiconductors, conduction band and valance band is formed due to e^- in s and p orbitals, respectively. The conduction band (s-band) shifts upward, and the valance band (p-band) shifts downwards[13]. Therefore, these bands never cross each other in ordinary materials. The band inversion in TIs is occurred due to the strong spin orbit coupling, which is responsible for the unique properties. In some materials, SOC is large, the p-band (valance band) shifts upward, and the s-band shifts downward direction. Due to this band shifting, the s and p band cross each other, and the normal band structure gets inverted,

which is called band inversion[5], [17]. The energy of the p-band (valance band) becomes higher than the energy of the s-band due to the band inversion. The point where bands are intersecting each other, these states are the conducting states which introduce the surface state. At this point, the bandgap is vanished at the surface state and becomes the metallic surface state.

The spin up and spin down e^-s encounter at the TSS in alternate effective fields which leads them to transmit in the reverse direction. This phenomenon is known as spin momentum locking. This is useful from the application point of view. The spin state depends on the applied current at the surface. If the direction of the applied current is reversed, the spin state is also reversed. We can implement this property in data storage and switching device application. The most intriguing property of spin moment locking in TIs is that the e^- motion remains unperturbed from backscattering. To understand this phenomenon, let us consider a spin up e^-, which is propagating in the forward direction, and the spin of the electron is locked with its momentum. Backscattering can occur if the spin up e^- flips in spin-down e^-, which is impossible because of the unavailability of the opposite spin state. However, backscattering can occur if TRS is broken (in case of magnetic impurity). Thus, the spin momentum locking and TRS both preserves the robustness of TSS and does not allow the backscattering. However, it is noteworthy that the above discussion is only applicable for odd no. of forwarding (or backward) moving channels. Though, backscattering can occur if even no. of channels.

1.5.7 Quantum Anomalous Hall Effect (QAHE)

In the nonmagnetic materials, the Hall voltage is proportional to the applied magnetic field due to Lorentz force, as we have discussed earlier in detail. The slope of the curve displays linear field dependence and is governed by the type and charge density of

carriers. After the discovery of the ordinary Hall effect (OHE), Hall carried out the same experiments for the ferromagnetic materials and observed an unusual large slope at a low magnetic field. Later, it was found that such type of unusual behaviour is originated due to spontaneous magnetization of the ferromagnetic materials. This additional effect with the ordinary hall effect is known as anomalous Hall effect (AHE) and is shown in figure 1.13. As a ferromagnetic material can show spontaneous magnetization even in the absence of magnetic field, the anomalous Hall effect (AHE) can be measured in the absence of magnetic field. It is believed that spin-orbit coupling (SOC) plays a major role in the presence of anomalous Hall effect (AHE), but the exact reason is still not clear. Other reasons such as skew scattering or side jump of carriers (extrinsic mechanisms) and intrinsic mechanisms may also be responsible for the AHE[18]. The quantum mechanical version of the anomalous Hall effect is known as the quantum anomalous Hall effect (QAHE). Soon after the discovery of the quantum anomalous Hall effect, it was realized that the theory which is used to explain the QHE might be used in the explanation of QAHE in the magnetic materials.

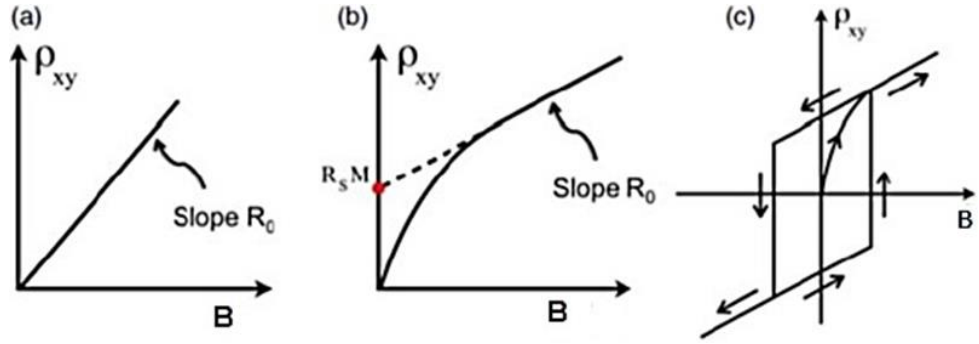

Figure 1.13: The variation of Hall resistivity ρ_{xy} with the applied magnetic field B. (a) ordinary Hall effect (b) anomalous Hall effect (AHE) (c) measured hysteresis loop from quantum anomalous Hall effect (QAHE)(Adapted from[18]).

1.5.8 Shubnikov-de Haas (SdH) Oscillations

When 2D electron gas is subjected to a strong magnetic field at low temperature, energy levels are split into discrete energy levels called Landau levels, which we have discussed earlier in section (1.5.3). Due to the effect of a strong magnetic field, the electrons are localized and move in a cyclotron motion with a frequency $\omega_c = eB/m^*$, where e is the charge of the electron, B is the magnetic field and m^* is the effective mass of electrons. The energy value of landau levels can be written in equation (1.18) as;

$$E_n = (n + \frac{1}{2}) \hbar\omega_c$$

As the value of the magnetic field is increased, the separation between the Landau levels is also increased. As a result of a continuous increase in the magnetic field, the position of the Landau level varies. Therefore, for a concise time interval, the Fermi level lies in the Landau level, and electrons jump from the occupied level (below the Fermi energy) to the unoccupied level (above the Fermi energy). In this process, the electrons get scattered in that Landau levels, and a prominent peak emerges in the resistivity vs magnetic field graph. If the Fermi level stays between the two Landau levels, no scattering occurs; as a result, no peak appears in the R vs B graph. Hence the oscillations are observed in the resistivity and called Shubnikov-de Hass (SdH) oscillation. If the oscillations are observed in magnetization vs magnetic field curve, these oscillations are known as de Hass-van Alphen (dHvA) oscillations. Shubnikov-de Hass oscillations are observed only for the perpendicular magnetic field in 2D electron gas, while in 3D electron gas, SdH oscillations can be observed in any direction. SdH oscillations give information about the Berry phase[19]. With the help of SdH oscillations, we can determine the effective mass, surface carrier density, dingle temperature, quantum mobility as well as Fermi surface can be mapped.

1.5.9 Weak Localization (WL) and Weak Antilocalization (WAL) Effects

In experiments, the delocalization of e^- was explained by a phenomenon called weak antilocalization (WAL). This effect originates from the π Berry phase due to which a destructive quantum interference between time-reversed loops formed by scattering trajectories. The destructive interference can prevent the backscattering of e^-. By decreasing temperature, the value of conductivity is increased because decoherence mechanisms are reduced at low temperatures. The interference and conductivity both can be destroyed by the magnetic field. Therefore, the signature of WAL is a negative magnetoconductivity which can be easily observed in many topological insulators. The WAL phenomenon is associated with the surface state of the TIs[13], [20]. It can be observed only at low magnetic field and low temperature. It is verified that due to spin-orbit scattering, quantum interference changes from constructive to destructive, while in WL effects, e^-s are localized due to constructive interference between two time-reversed paths of the e^- wave function, which suppress their ability of current transport.

In the experiments, with the help of HLN formula[21], the WAL and WL effect for 2D system was analyzed. The HLN equation can be expressed as;

$$\Delta\sigma = \sigma(B) - \sigma(0) = \frac{\alpha e^2}{\pi h}\left[\psi\left(\frac{1}{2}+\frac{h}{8\pi eBl_\varphi^2}\right) - ln\left(\frac{h}{8\pi eBl_\varphi^2}\right)\right] \quad (1.19)$$

Where l_φ represents phase coherence length, ψ is a digamma function and $\boldsymbol{A = \frac{\alpha e^2}{\pi h}}$ represents the number of conduction channel, and α is the prefactor value.

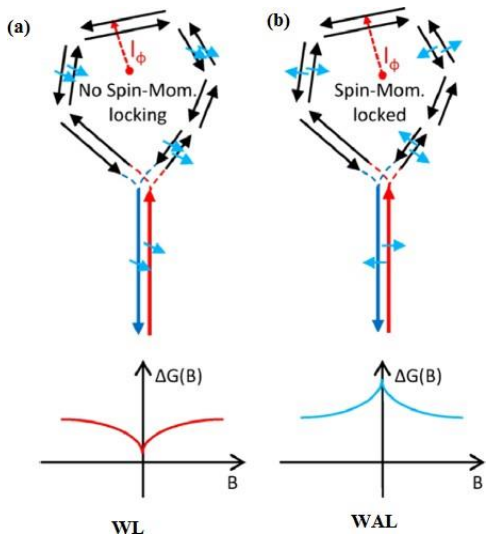

Figure 1.14: (a) The two time-reversed scattering loops without spin-momentum locking exhibiting weak localization in magnetoconductivity (ΔG (B)). (b) The two time-reversed scattering loops with spin-momentum locking exhibited weak antilocalization in ΔG (B) (Adapted from [13]).

1.6 Historical Developments of 2D and 3D Topological Insulators

1.6.1 First 2D topological insulator HgTe

Theoreticians predicted the existence of the QSH state in HgTe quantum well sandwiched between the layers of CdTe. In the year 2006, Bernevig reported this heterostructure of HgTe having thickness $d_{HgTe,}$ which is sandwiched between the two thin layers of CdTe with equal thickness d_{CdTe}. The thickness of HgTe plays a major role in the band structure of this heterostructure[1], [13], [14]. The electronic band structure of this heterostructure at the Γ point has an inverted band structure. The confinement energy increases as the value of d_{HgTe} decreases, due to which the energy band shifts. When the thickness d attains the critical value, i.e., $d = d_c$, QSHE emerges without any external magnetic field. The heterostructure of CdTe/HgTe/CdTe and the band structures of HgTe, CdTe is shown in figure 1.15. With the variation of the width 'd' of the quantum well, the corresponding band structure is shown in figure 1.15. The band inversion at the

Γ point has occurred after the critical width d_c. 1-D helical edge state comes to light, and band inversion takes place at the boundaries of 2-D quantum well. At the critical thickness d_c (6.3nm), the bandgap vanishes, and the Dirac cone touches each other at a point called Dirac point. The experimental verification of the QSHE in HgTe quantum wells system has been reported. This fact is also supported by the experimental evidence for the spin polarization of the QSH edge state.

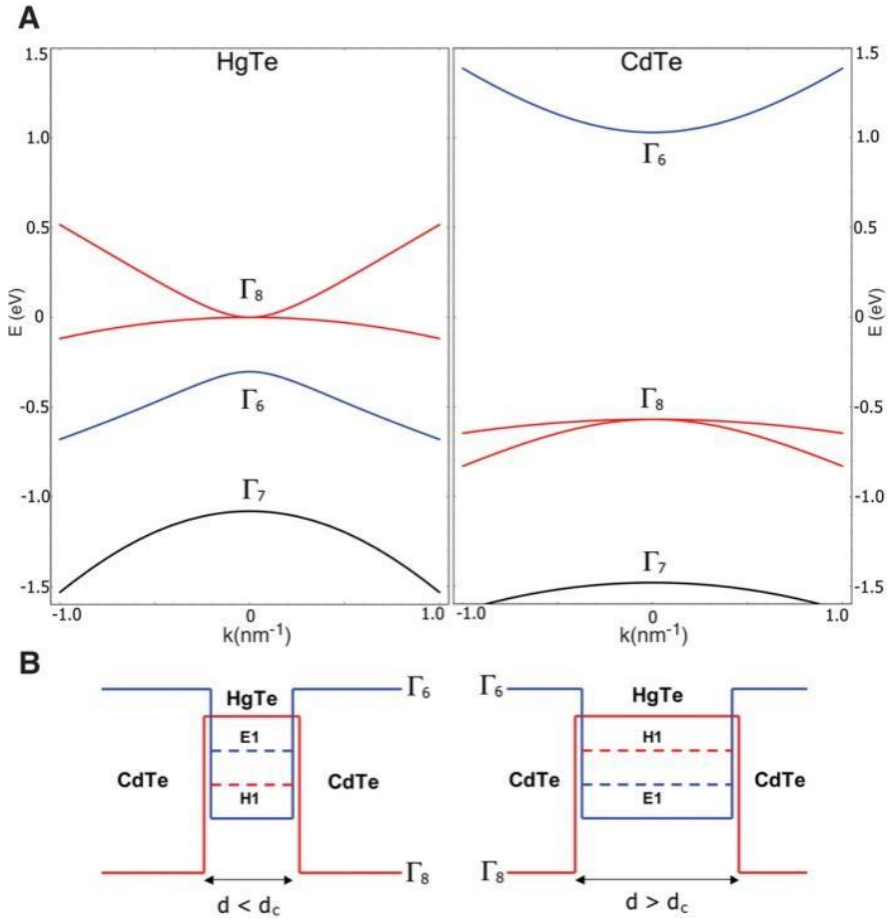

Figure 1.15: (a) bulk energy bands for HgTe and CdTe at Γ point (b) CdTe/HgTe/CdTe quantum well in normal regime $d < d_c$ and in inverted regime $d > d_c$ (Adapted from [13]).

1.6.2 3D Topological Insulators

After the development of 2D topological insulator, one can evolve the concept of 3D topological insulator. Moore and Balents[22], Roy[23] and Fu, Kane and Mele[24] established the concept of 3D topological insulators. 2D topological systems have conducting edges, whereas 3D topological systems have conducting surface state. In 3D TIs, the bandstructure of the surface state can be characterized as a 2D state with the band dispersion of a single Dirac cone. Strong topological insulators have odd no. of Dirac cones. 3D TIs possess four Z_2 topological invariants (υ_0, υ_1, υ_2, υ_3), where υ_0 is associated with strong topological invariant and υ_1 - υ_3 belongs to the weak topological invariant. The strong topological insulator $\upsilon_0 = 1$ follows that there must be odd no. of Dirac cones present at the surface of topological insulators. The spin-momentum locking in the perpendicular direction of the surface state is the most intriguing property of the 3D topological insulators. The state has momentum K and –K possesses opposite spins, i.e., up spins are propagating in +x direction and down spins are moving in –x-direction. Therefore, the backscattering does not occur at the surface state of the topological insulator and the surface state becomes robust.

1.6.3 The First 3D Topological Insulator $Bi_{1-x}Sb_x$

Immediately after the experimental verification of the existence of QSH state in 2Din HgTe quantum well, in the year 2008, Hsien et. al[25] reported the first experimental evidence of the presence of 3D TI state in the material $Bi_{1-x}Sb_x$. The 3D TIs needed ARPES measurement to study the surface band structure. Zahid Hassan's group experimentally explained the presence of QSH in 3D $Bi_{1-x}Sb_x$ by using ARPES[25]. In 3D materials, understanding the charge transport is very difficult, unlike the 2D materials as a reason of bulk effects. This makes it very ambiguous to establish

the topological signature at the surface state. ARPES is a perfect technique, can be utilized to investigate the surface states which are topologically protected. In ARPES, a photon is used to eject the electron from the crystal to find the surface and bulk electronic structure by examining the ejected electron momentum. ARPES allows separation of the bulk band structure from the surface state because surface states do not disperse transverse to the surface[1]. A strong topological insulator exhibits a linear dispersion relation. In this, the metallic surface state crosses the Fermi level at an odd no. of points. The ARPES spectrum of $Bi_{1-x}Sb_x$ depicts in the figure. 1.16, where the surface state crosses Fermi energy five times. According to Kramer's theorem, such type of an odd number of crossings suggests the topologically protected states in $Bi_{0.9}Sb_{0.1}$. However, in $Bi_{1-x}Sb_x$, observing the topological surface state is very complicated in nature[1]. Soon after the experimental discovery of $Bi_{1-x}Sb_x$, in 2009, Zhang et al.[26] predicted some chalcogenide compounds (A_2B_3) as 3D TI theoretically by using *ab initio* functional theory. The non-trivial surface state and calculated bulk bandgap of Bi_2Se_3, Sb_2Te_3 and Bi_2Te_3 have been shown in figure 1.16. The band structure can be easily seen in these materials which are experimentally verified by using ARPES. In figure 1.16, the linear dispersion at the surface state can be seen in the ARPES spectrum of Bi_2Se_3, and the presence of a Dirac cone in the band structure confirmed it as a TI.

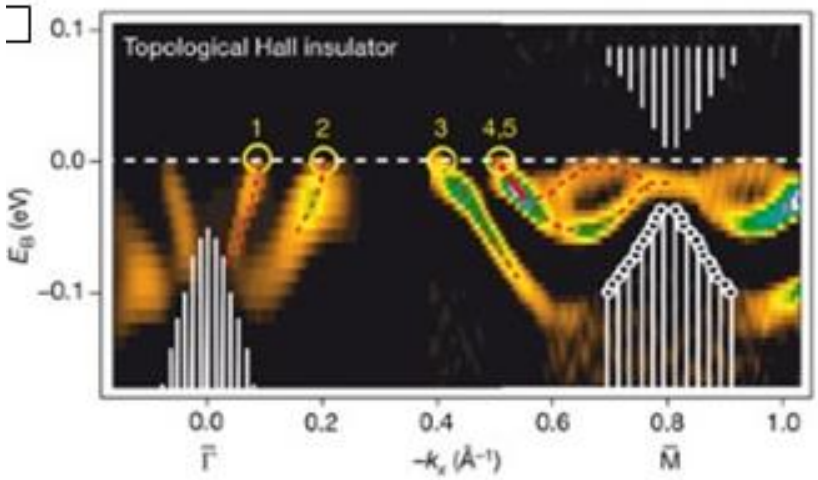

Figure 1.16: The surface band dispersion second-derivative image of $Bi_{0.9}Sb_{0.1}$. there are five crossing between ┌ and M which confirms topological non-trivial surface state (Adapted from [6]).

1.6.4 New materials Bi_2Se_3, Bi_2Te_3 and Sb_2Te_3

Bi_2Se_3 is the most extensively studied TI till date, however it is not an ideal material and has several imperfections due to which it is ambitious to retrieve the topological surface state in a transport experiment.

In figure 1.17, non-trivial state of Bi_2Se_3, Sb_2Te_3 and Bi_2Te_3 can be seen clearly. The calculated band gap for Bi_2Te_3 is 100mev, for Sb_2Te_3 260mev and 300mev for Bi_2Se_3. Similar to $Bi_{1-x}Sb_x$, Bi_2Se_3, Bi_2Te_3 and Sb_2Te_3 also possess the same strong topological invariant; hence a lot of studies has been done on these materials. All these materials are pure in nature, unlike $Bi_{1-x}Sb_{x,}$ which is an alloy. Therefore, these materials can be prepared in high purity[6], [27]. Moreover, in these materials, topological surface state can be easily seen in the ARPES spectrum, as well as they have a large bandgap (as mentioned above) even at room temperature. These properties make them a good Topological insulator, due to which they are the most studied TI system.

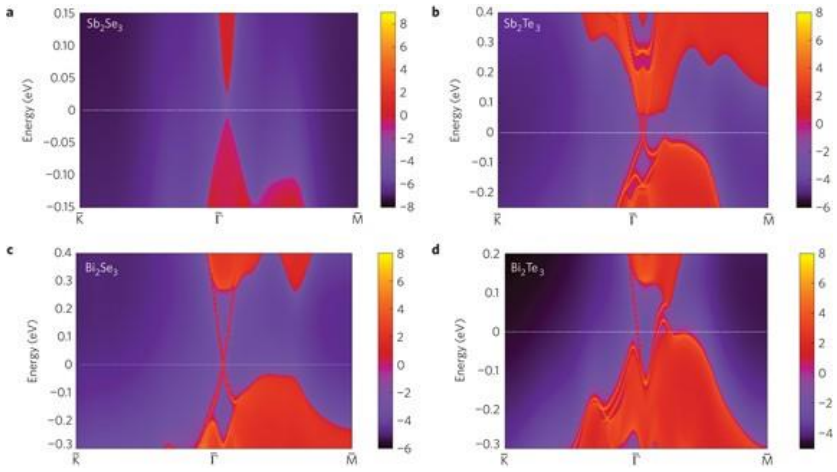

Figure 1.17: Calculated band structure of Sb_2Se_3, Sb_2Te_3, Bi_2Se_3 and Bi_2Te_3 by ab initio density functional theory. Red represents occupied bulk and surface states, and blue signifies bulk band gap[6].

1.6.5 Crystal structure and Symmetry Properties

Bi_2Se_3, Bi_2Te_3 and Sb_2Te_3 are layered materials and belong to the rhombohedral crystal structure with R-3m space group. Let us consider Bi_2Se_3 as an example. Figure 1.18 shows the crystal structure of Bi_2Se_3. The structure has five atoms per unit cell which is ordered in Se1-Bi1-Se2-Bi1'-Se1' layered manner along the c-axis and called quintuple layers. The layers have covalent bonding, and in the quintuple layer, the weak Van Der Waals forces exist. The thickness of one quintuple layer is 1nm. Each layer of atoms makes a triangle lattice known as tetradymite-type lattice. The triangle layers are ordered A-B-C-A-B-C type of arrangement along the z-axis. In one unit cell, there are two Bi atom and three Se atoms in which two equivalent Bi (Bi1 and Bi1') atoms, two equivalent Se atoms (Se1 and Se1') and one equivalent Se atom (Se2) are present.

In these types of crystal structures, four types of symmetries exist.

1- Threefold rotation R3 along the z-direction: such type of symmetry can be created due to the following transformations:

$X \rightarrow x\cos\theta - y\sin\theta$, $x \rightarrow x\sin\theta + y\cos\theta$ and $z = z$, where $\theta = 2\pi/3$

2- Twofold rotation R2 along the x-direction: in this transformation Bi1-Bi1', Se1-Se1' and Se2-Se2 have the coordinate transformation $x \rightarrow x$, $y \rightarrow -y$ and $z \rightarrow -z$. Under this transformation, the layers Bi1(Se1) and Bi1'(Se1') interchange their positions.

3- Inversion Symmetry: In such type of symmetry Bi1 → Bi1 and Se1 → Se1'; Se2 → Se2 takes place and the coordinates changes as $x \rightarrow -x$, $y \rightarrow -y$ and $z \rightarrow -z$.

The strong SOC drives a band inversion at the Γ point in the Brillouin zone. figure 1.14 displays the schematic change in the atomic energy levels of Bi_2Se_3 and the effect of crystal field splitting and SOC on the energy eigenvalues at the Γ point as calculated by Zhang et al. [28]. The strong SOC drives a band inversion at the Γ point in the Brillouin zone. figure 1.19 displays the schematic change in the atomic energy levels of Bi_2Se_3 and the effect of crystal field splitting and SOC on the energy eigenvalues at the Γ point as calculated by Zhang et al. [28]. The outermost configuration of Bi and Se atoms are $6S^2\ 6p^3$ and $4S^2\ 4p^4$ respectively. Since a unit cell consists two Bi and three Se, and the outermost cell of each atoms contain three p orbitals p_x, p_y and p_z, so there are total fifteen p orbitals in a unit cell of Bi_2Se_3.

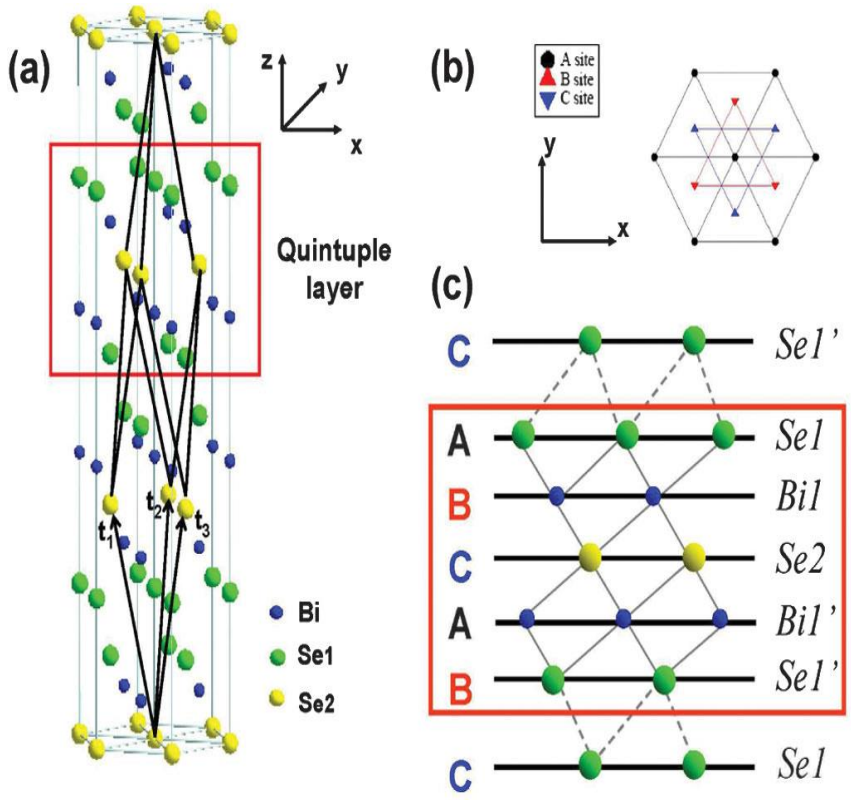

Figure 1.18: (a) Crystal structure of Bi_2Se_3, the red box shows single quintuple layer (b) shows that three different A, B, and C sites are assigned to triangular lattice in one quintuple layer (c) Se and Bi atoms are arranged in a sequence in quintuple layer. (Adapted from [28])

In stage I, Bi energy levels are pushed up and Se levels are pushed down because of chemical bonding. In stage II, due to crystal field splitting Bi energy level splits in to two levels with different parity i.e., one odd, one even denoted as $P1^{-}_{xyz}$, $P1^{+}_{xyz}$, respectively. In contrast, Se energy levels split into three states with different parity i.e., two odd, one even denoted as $P0^{-}_{xyz}$, $P2^{-}_{xyz}$ and $P2^{+}_{xyz}$ respectively. In stage III, after taken SOC into consideration the energy level which is below the E_F moves to upside and the level which is above the E_F moves downward. Therefore, Strong SOC leads to band inversion in Bi_2Se_3 system.

When a magnetic impurity is doped in a TI then unusual magnetotransport effects are noticed in these magnetically doped TIs due to broken of TRS. Various 3d-transition metal

elements doped magnetic TIs have been investigated theoretically and experimentally [27], [29]. Mn doped Bi_2Te_3 [30] clearly exhibited the ferromagnetic ordering at 12 K for doping concentration up to 9%. On the other hand, Fe and Mn doped Bi_2Se_3 do not show the ferromagnetic ordering, however a small surface state gap opened at the DP as confirmed from the ARPES measurement [27]. Therefore, it is necessary to investigate various magnetic topological insulators for better understanding and technological applications.

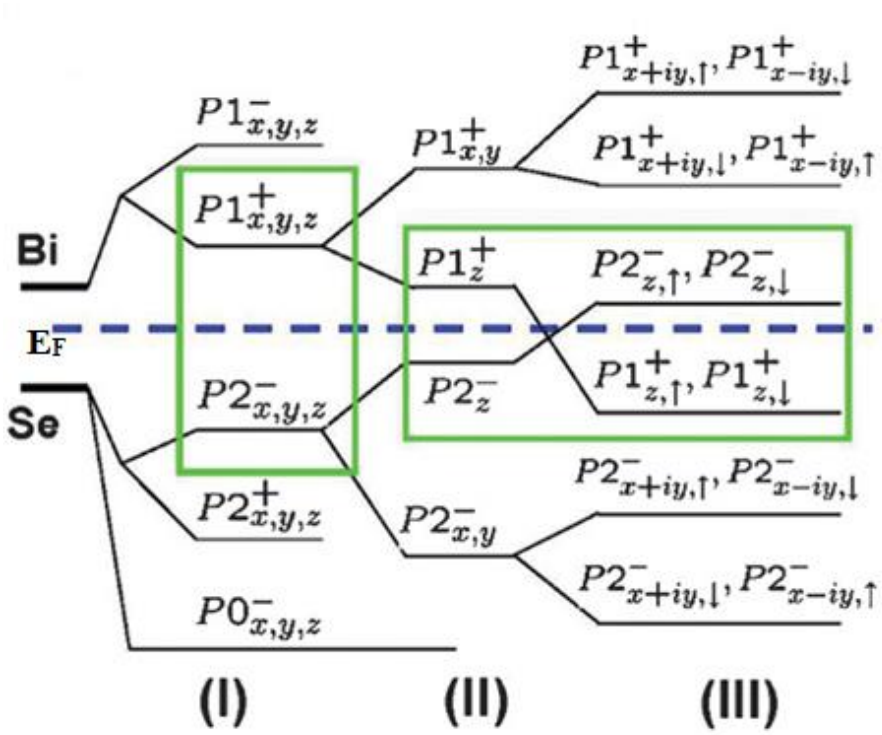

Figure 1.19: Schematic picture of the band inversion of Bi and Se p orbitals in Bi_2Se_3 at the Γ point. Stage I represents the effect of chemical bonding, Stage II represents the crystal field splitting, Stage III represents the effect of SOC. (Adapted from [28])

Moreover, superconductivity can also be induced in TIs by creating either internal chemical pressure on doping or by applying external pressure. However, only few topological superconductor systems have been discovered so far. Cu-intercalated Bi_2Se_3 is an example of internal chemical pressure induced topological superconductor systems [31]. Whereas,

The external pressure induced superconductivity has been observed in pure Bi_2Te_3 with T_c of ~3 K when external pressure applied in between 3 to 6 GPa [32].